A programmable pulse UWB transmitter with 34% energy efficiency for multichannel neuro-recording systems

Henrique Miranda and Teresa H. Meng
Electrical Engineering Department, Stanford University
Stanford, CA 94305, USA
Email: hmiranda@stanford.edu, thm@stanford.edu

***Abstract*—This paper describes configurable, 3.6 to 7.5 GHz pulse UWB transmitter IC targeted for neurological implants with high data rate requirements. Each cycle of the RF pulse is digitally programmable in amplitude and duration, enabling a very flexible shaping of the transmitted PSD signal, without the use of an output filter. The transmitter achieves a maximum of 34% of energy efficiency when drawing 8.5 pJ/bit from the supply, with 13 μW of constant static power. This transmitter was implemented in 65nm CMOS and measures 1.0 mm × 0.7 mm. A 32-channel recording experiment using this chip is also reported.**

Keywords: Ultra-wideband transmitter, wireless high-rate biotelemetry, programmable UWB waveform

I. Introduction

There has been an increasing need for high data rate wireless transmitters in biomedical applications such as neural prosthesis, where data from tens to hundreds of electrodes need to be recorded and transmitted to an external controller for extended periods of time. Since the supply energy available in these applications is scarce, the transmitter power consumption and efficiency are the most important design parameters [1]. Pulse UWB transmission is particularly suited for this application since it does not require the generation of a carrier signal and the circuitry can be operated in a very low duty cycle regime. This paper introduces a pulse UWB transmitter IC that can achieve 34% of energy efficiency, η_E, defined as the ratio of transmitted RF pulse energy per bit, E_{RF}, to the active DC energy, E_{DC} ($\eta_E = E_{RF}/E_{DC}$). This IC was designed for transmitting data detected by a 96-channel neural electrode array. At 24 Mbit/s, the output waveform can be configured so that the total average power consumption of the chip, which includes all blocks except I/O drivers, is only 204 μW ($E_{DC} = 8.5$ pJ/bit) sufficient to cover a distance of 5 m with a custom designed receiver. The static power consumption of the transmitter is a fixed 13 μW. Another UWB transmitter for neuro-recording applications has been reported earlier [3] but it lacks the waveform reconfigurability feature provided by this UWB architecture. Advantages of this reconfigurability will be explored in the following sections.

II. Transmitter architechture

This UWB transmitter is based on a cascadable architecture whose basic element is the single pulse cell (Fig. 1). Each cell has a 3-bit programmable delay between input and output

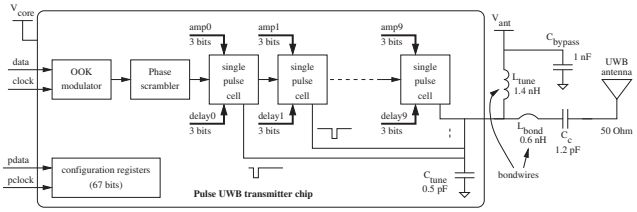

Fig. 1: Block diagram of the pulse UWB IC transmitter architecture

and it controls the duration of each cycle of the RF pulse. This delay is individually configured for each cell in the chain, forming a delay configuration vector (DCV). The number of cascaded cells defines the number of RF cycles, thus setting the maximum RF pulse duration and, consequently, the lowest pulse bandwidth. The chip includes 10 pulse cells that generate signals bandwidths larger than 450 MHz. The programmable delay cell schematic is shown in Fig. 2. The delay is controlled through the discharge rate of the MOS capacitor by three digitally controlled binary weighted parallel branches. The MOS capacitor is charged at a fixed slow rate through the PMOS device when the inverter returns to the initial state (absence of an OOK pulse). This delay control mechanism enables an approximate linear frequency dependency on the delay control numbers. The binary weighted antenna driver transistors (M1-M3) are turned on at the onset of the input rising edge, during half of the cell delay time (t1-t0). These transistors remain in the off state after the falling edge (t1), during which the state of the single pulse cell is reset, making it ready for the next bit transmission. All the antenna driver transistor drains are connected to a wideband resonator circuit

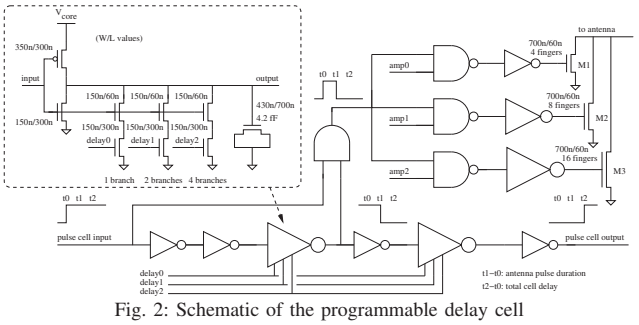

Fig. 2: Schematic of the programmable delay cell

978-1-4244-5760-1/10/$26.00 ©2010 IEEE

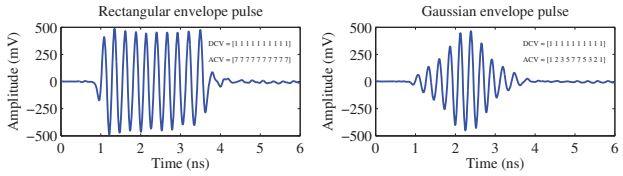

Fig. 3: Measured output pulse waveforms at 3.6 GHz for rectangular and Gaussian envelopes

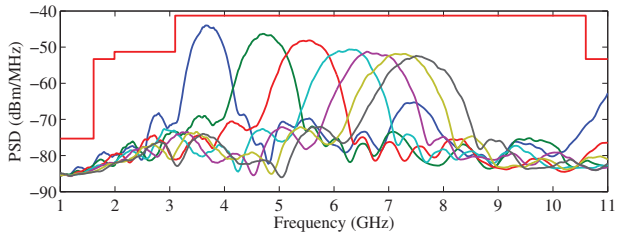

Fig. 4: Output PSD of the Gaussian pulse for all frequencies at V_{core} = 1.2 V and V_{ant} = 0.7 V.

formed by L_{tune}, a 1.4 nH bond wire, and an on-chip 0.5 pF capacitance, C_{tune}, in a wired or configuration (the parasitic capacitance of the driver transistors is included in C_{tune}). The loaded Q of this resonator is approximately unitary, which is a good compromise between waveform smoothing, frequency roll-off and pulse tail ringing.The off chip coupling capacitor (C_c) simultaneously removes the pulse DC component and resonates out the bond wire inductance L_{bond}. The combination of these two resonant circuits form a band pass response characteristic that is flat from 3.5 to 11 GHz (within a 3 dB variation.)

The antenna drive strength of each cell can be configured to one of eight levels in a linear scale, forming the amplitude configuration vector (ACV). This type of antenna driver arrangement constitutes an RF DAC where the amplitude of each individual cycle of the RF pulse can be digitally controlled, thus enabling a very flexible spectrum control. Fig. 3 shows two examples of measured output waveforms: a rectangular and a Gaussian envelope pulses. The PSDs of the Gaussian envelope pulse is shown in Fig. 4 for all transmitter frequencies, and they meet the indoor UWB FCC spectrum mask. This antenna driver scheme is also very power efficient since 1) there are no losses associated with scaled driver inverter stages commonly found in other UWB designs (e.g. crowbar currents) [2][3] and 2) no output BPF is required to meet the spectral mask, and therefore no RF energy is lost by this shaping filter [4]. The measured efficiency performance and the transmitted RF energy of the transmitter are depicted in Fig 5 for the rectangular and Gaussian pulse envelopes. The maximum efficiency is attained for V_{ant} of 0.75 V for both waveforms. The modulator uses the OOK method in which RF pulses are transmitted only for bit "1" in the input data stream. For balanced streams, this effectively halves the average power consumption of the chip (neglecting the static power consumption).The UWB OOK modulated signal contains discrete spectral lines that can limit the maximally usable RF power, since they will be the first to violate the spectrum mask as we increase the power level. In order to

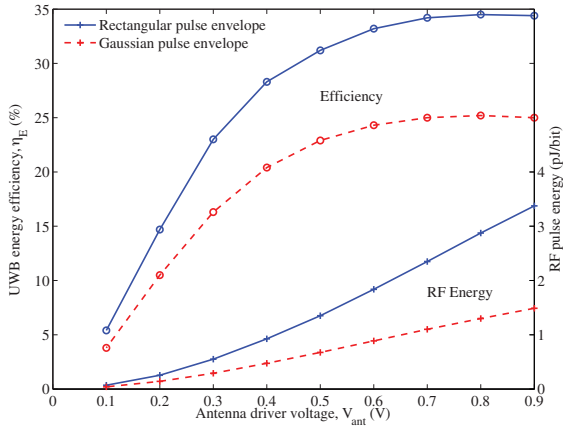

Fig. 5: Measured efficiency (η_E) and output RF energy vs antenna driver voltage V_{ant} for the rectangular and Gaussian profiles.

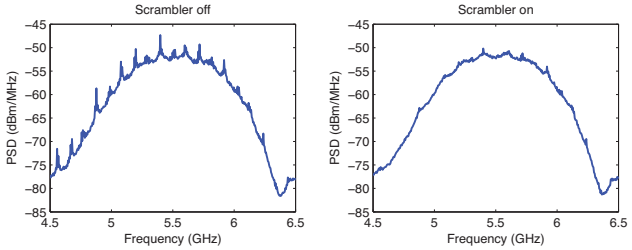

Fig. 6: Reduction of the spiky nature of the OOK spectrum by the phase scrambler.

suppress these spectral peaks, a pulse phase scrambler was inserted after the OOK modulator. A balanced PN sequence of length 128 generated by a complete LFSR drives a multiplexer, which adds either a delay of half RF cycle or no delay. The scrambler action can be verified by the spectrum shown in Fig. reffig:scrambler, where a 4 dB suppression of spectral peaks is achieved.

The chip was tested using a chip-on-board technique as depicted in Fig. 7, where the antenna interface wire bonding scheme is shown.

III. Experimental Measurements

The development of this chip is part of the Hermes, a project aimed at recording and transmitting neural activity from brain implanted electrode arrays for neuroscience research applications. The previous generation, named HermesD [5], was

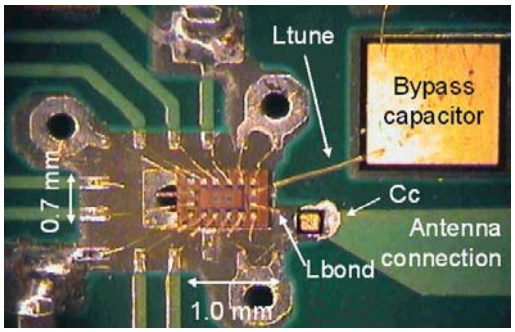

Fig. 7: Photograph of the chip assembly

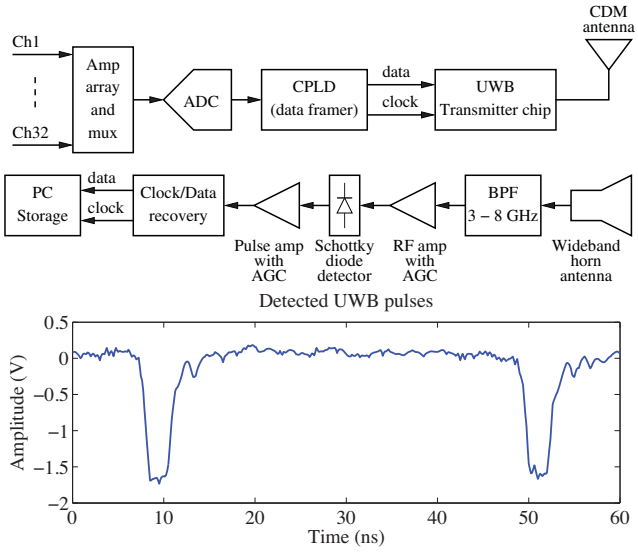

Fig. 8: Top: block diagram of the UWB based recording setup (HermesE); bottom: waveform at the output of the pulse amplifier for a receiver separation of 5 m.

entirely based on of-the-shelf components, and because of that, it was not very power efficient. Its global power consumption is 142 mW, with 30 mW dedicated for its transmitter. HermesE, the next generation, will contain two custom designed ICs: a 96-channel analog interface circuit (AIC) that still in development (includes the amplifier array, A-to-D conversion and multiplexing) and the UWB transmitter described in this paper. The custom based solution enables a tremendous power reduction, to about 8 mW total, with less than 1 mW allocated to the transmitter.

A. Device Validation

To validate the performance of this chip, a neural recording experiment was setup as shown in Fig. 8. On the transmitter side, the analog and digital processing sections were imported from the HermesD system (while the custom AIC is not completed). These blocks provide amplification, A-to-D conversion and data framing for 32 neural channels, at a rate of 24 Mbit/s. The data and clock are applied to the UWB transmitter input, while a 3-11 GHz circular dish monopole (CDM) of 19 mm in diameter is used as the antenna. The UWB chip was set as follows:

- $V_{\text{core}} = 1.2$ V; $V_{\text{ant}} = 0.8$ V
- ACV = [7 7 7 7 7 7 7 7 7 7] (rectangular envelope)
- DCV = [2 2 2 2 2 2 2 2 2 2] (4.8 GHz RF pulse)

For this configuration, the measured power consumption of the chip core was 217 µW, of which 13 µW is static power.

The UWB receiver is based on a fast Schottky diode detector (Pasternack PE8004), which is able to provide sub-ns rise and fall times in a 50 Ω impedance system. The pre and pos detection level controlled amplifiers ensure a steady detected signal with sufficient amplitude for reliable operation of the clock/data recovery circuitry (the same used in HermesD). The detected signal at the output of the pulse amplifier is shown in the plot of Fig. 8 when the reveiver is 5 m away from the transmitter. The pulse waveform exhibit an SNR of about 25 dB, providing error free operation. Multipath effects would show as trailing pulses and they do not reppresent a problem as long as they lie inside the bit period (42 ns in this experiment).

B. Neural data recordings

The HermesE system was used to obtain neural data *in vivo*. One adult male rhesus macaque was implanted with a 96-electrode array (BlackRock Microsystems Inc., Salt Lake City, UT [6]) using standard neurosurgical techniques similar to those described in [7] 25 months prior to the current study. The electrode array was implanted in a region spanning the arm representation of the dorsal aspect of premotor cortex (PMd) and primary motor cortex (M1), as estimated visually from local anatomical landmarks. All of the surgical procedures were approved by Stanford University's Institutional Animal Care and Use Committee (IACUC.) The prototype was tested inside an experimental room while the animal was seated in a primate chair. All 32 channels of neural data were received wirelessly at a distance of 3 m.

The neural signals acquired during one recording session are shown in Fig. 9. In order to produce these 32 waveforms, the following procedure was followed: first, a second order high-pass Butterworth filter with a 250 Hz cutoff frequency was applied to each of the channels to isolate the neural spike band. Then, to find neural spikes in the data, a threshold of three times the RMS value was set. If this value was crossed, a snippet of data around this time was extracted and a shape heuristic was applied. This heuristic filters for events in which the negative deflection is followed by a positive deflection. To reduce the timing jitter in each waveform snippet that is created by thresholding a discrete signal, the snippets are upsampled by a factor of 8, center-of-mass aligned, and downsampled to the original sampling rate. Finally, action potentials extracted from the 5 seconds of data are overlaid on top of each other for each corresponding channel plot.

The root mean squared (RMS) of each channel was calculated from 120 seconds of recorded data by taking the standard deviation of the spike band. Across all 32 channels, the RMS has a mean of 15.9 µV and a standard deviation of 4.9 µV. The distribution of RMS values is similar to the distribution measured on the same electrodes with a commercially available wired recording system, Cerebus (Blackrock Microsystems Inc., Salt Lake City, UT), with a mean of 17.2 µV and a standard deviation of 5.5 µV.

IV. Conclusion and Applications

This paper presented a very low-power UWB transmitter targeted for multichannel neuro-recording applications. It is currently being integrated into a 96-channel wireless neural recording system named HermesE, to be used with freely moving monkeys. A preliminary recording experiment using this UWB IC in a 32-channel setup was successfully demonstrated. The custom built receiver was placed 3 m away from the monkey subject and data was collected into a PC.

This transmitter architecture provides a very versatile way of controlling the transmitted PSD, just by changing the ACV and

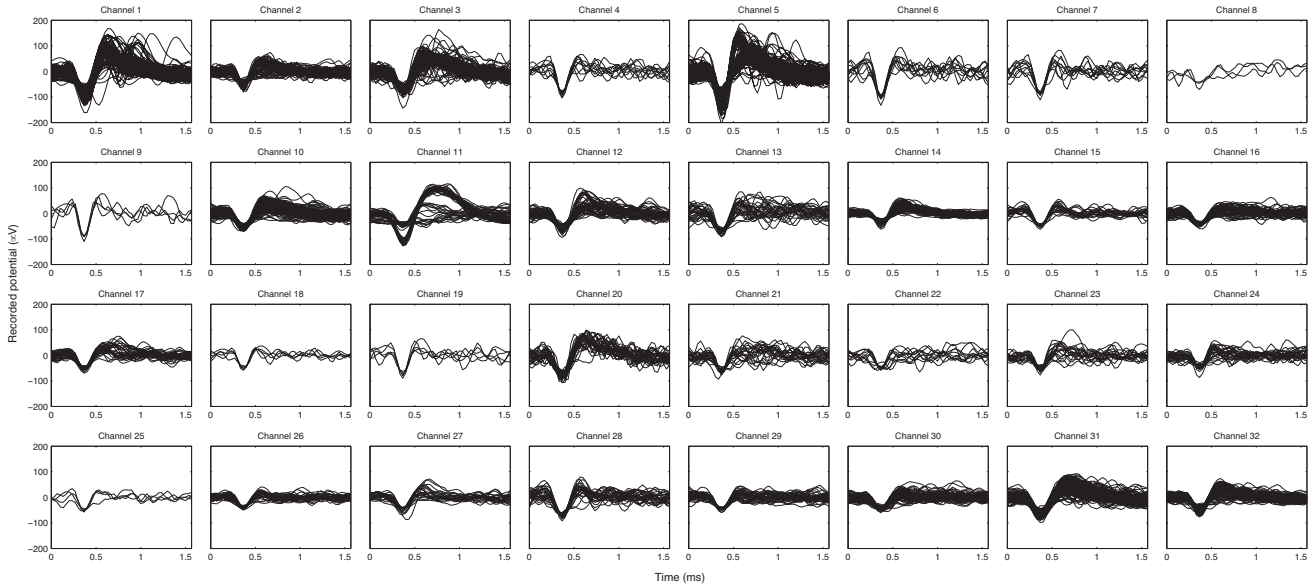

Fig. 9: UWB Wireless *in vivo* recording of neural activity of a rhesus macaque. Plots show the extracted action potentials of 5 s of neural activity for all 32 channels.

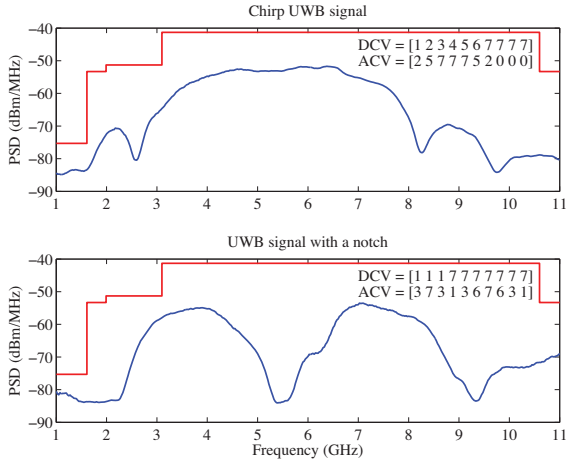

Fig. 10: A 3 to 8 GHz UWB pulse with spectrum suppression in the 5 to 6 GHz band.

DCV vectors. One possible example is the ability to generate frequency chirp signals. Fig. 10 (top) shows a 3 to 8GHZ chirp where the bandwidth is decoupled from pulse duration, making it possible to improve the signal detectability in receivers that use pulse compression techniques. Another spectrum control example is the possibility to suppress a portion of the spectrum to minimize interference with other services like WLAN in the 5.8 GHz ISM band. Fig. 10 (bottom) shows the measured spectrum of a 3 to 8 GHz pulse in which the 5 GHz to 6 GHz band was suppressed by appropriately setting the ACV and DCV vectors. The spectrum control mechanism also enables the transmission in multiple spectrum bands, providing frequency diversity to increase the communication robustness in severe multipath channels. Also, these vectors can be configured to "pre-distort" the transmitted waveform to compensate for antenna gain variations. This is especially important for biological implants that use UWB antennas, since the surrounding tissues usually cause a frequency dependent antenna behavior.

ACKNOWLEDGMENT

We thank Mackenzie Risch for expert surgical assistance and veterinary care, Stephen Ryu for expert neurosurgical leadership, Vikash Gilja, Paul and Boris Murmann for technical consultation, Rachel Kalmar and Zuley Rivera for animal training and care. The authors also acknowledge the support of the Focus Center for Circuit & System Solutions (C2S2), one of five research centers funded under the Focus Center Research Program, a Semiconductor Research Corporation Program, the Rethinking Analog Design (RAD) initiative at Stanford University, and TSMC for the chip fabrication.

REFERENCES

[1] C. A. Chestek, V. Gilja, P. Nuyujukian, S. I. Ryu, K. V. Shenoy, R. J. Kier, F. Solzbacher, and R. R. Harrison, "HermesC: RF Wireless Low-Power Neural Recording System for Freely Behaving Primates," in *IEEE International Symposium on Circuits and Systems*. IEEE, May 2008, pp. 1752–1755.

[2] D. Wentzloff and A. Chandrakasan, "A 47-pJ/pulse 3.1-to-5GHz all-digital UWB tranmitter in 90nm CMOS," in *ISSCC Dig. Tech. Papers*, Feb 2007, pp. 118–119.

[3] e. a. M. Chae, "A 128-Channel 6mW Wireless Neural Recording IC with On-the-Fly Spike Sorting and UWB Transmitter," in *ISSCC Dig. Tech. Papers*, Feb 2008, pp. 146–147.

[4] e. a. V. Kulkarni, "A 750 Mbit/s, 12 pJ/b, 6-to-10 GHz CMOS IR-UWB transmitter with embedded on-chip antenna," *IEEE J. Solid-State Circuits*, vol. 44, no. 2, pp. 394–403, Feb. 2009.

[5] H. Miranda, V. Gilja, C. A. Chestek, K. V. Shenoy, and T. Meng, "A high-rate long-range wireless transmission system for multichannel neural recording applications," in *IEEE International Symposium on Circuits and Systems*, Taipei, Taiwan, May 2009, pp. 1265–1268.

[6] E. M. Maynard, C. T. Nordhausen, and R. A. Normann, "The Utah intracortical electrode array: a recording structure for potential brain-computer interfaces," *Electroencephalography and Clinical Neurophysiology*, vol. 102, no. 3, pp. 228–239, Mar. 1997.

[7] N. Hatsopoulos, J. Joshi, and J. G. O'Leary, "Decoding continous and discrete behaviors using motor and premotor cortical ensembles," *J. Neurophysiol.*, vol. 92, pp. 1165–1174, 2004.